Biophysical Journal, Volume *112*

Supplemental Information

Mechanical Characterization of Microengineered Epithelial Cysts by Using Atomic Force Microscopy

Yusheng Shen, Dongshi Guan, Daniela Serien, Shoji Takeuchi, Penger Tong, Levent Yobas, and Pingbo Huang

Linear isotropic poroelasticity and power-law models

The force relaxation of MDCK II cysts after a step displacement of the cyst surface was analyzed using the linear isotropic poroelasticity theory (1,2) and the power-law model (3), as described previously. Briefly, we adopted an approximate analytical solution for the indentation of a poroelastic infinite half-space by a colloidal indentor, as given below:

$$\frac{F(t)-F_f}{F_i-F_f} = 0.491e^{-0.908\sqrt{\tau}} + 0.509e^{-1.679\tau}. \quad (1)$$

Here, $\tau = D_p t/R_1\delta$ denotes the characteristic poroelastic time required for an initial force F_i to relax to F_f under a constant indentation. R_1 denotes the effective radius of the probe and δ is the indentation depth. For measuring the poroelastic diffusion coefficient D_p, Eq. 1 was used to fit our force-relaxation data.

For the fitting of the linear regime (in log-log scale) of the force-relaxation curves to the power-law model, we used Eq.2,

$$\sigma = \varepsilon_0 K_0 t^{-\beta}, \quad (2)$$

to obtain the power-law exponent β.

Supporting Figures

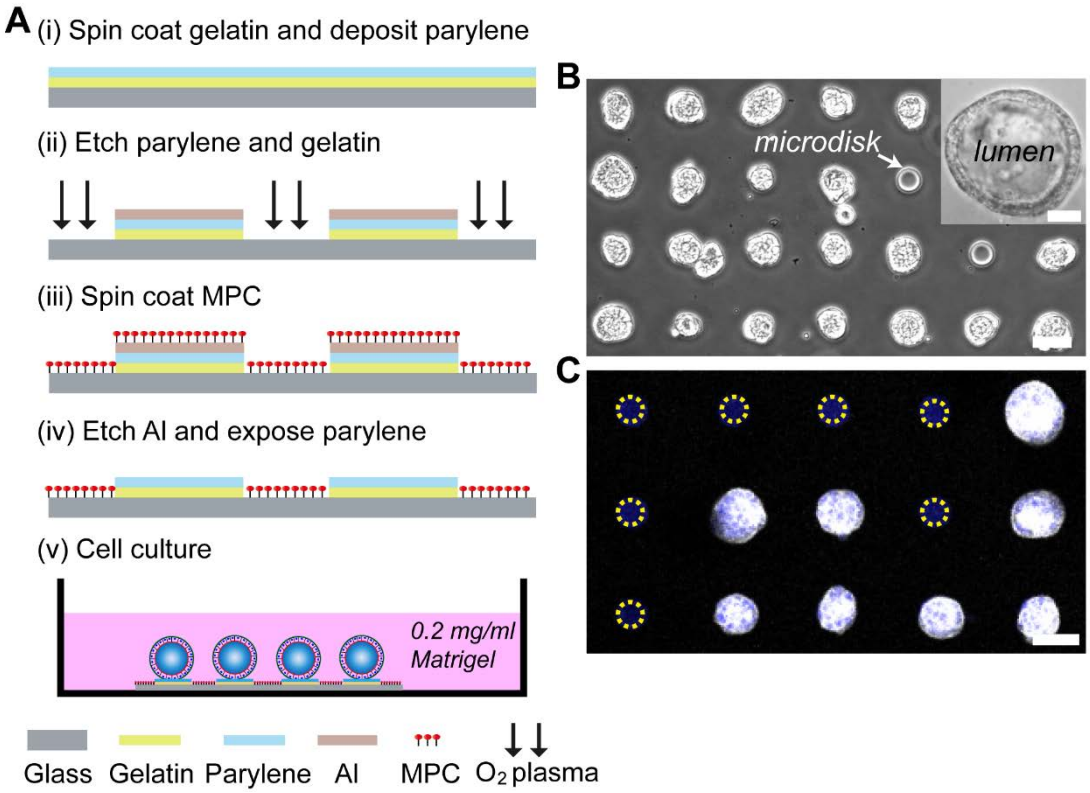

Figure S1 Microdisk fabrication and cyst-array generation. (*A*) Schematic of the parylene based microdisk fabrication process and the gel-free culture method. (*i*, *ii*) After spin-coating of gelatin (<0.05%, w/v, type A, Sigma-Aldrich) at 2000 rpm for 30s on plasma-treated glass and depositing the parylene film (~3 μm thick, LABCOTER PDS2010, Specialty Coating Systems, USA), standard photolithography with photoresist (S1818G, Shipley) was used to pattern an aluminum layer as a partial mask and O_2 plasma etching (20 sccm, 50 W, for 6 cycles of 10 min, RIE-10NR, SAMCO, Japan) was used to produce the microdisks at the region defined using the aluminum mask. (*iii*, *iv*) The regions without microdisks were passivated with the MPC polymer to prevent protein and cell adhesion by spin-coating MPC at 2000 rpm for 30 s, 20–30 min drying under ethanol-saturated atmosphere and further drying at 70°C for 4 h and lift-off by sacrificial aluminum etching before cell culture. (*v*) MDCK-II cells were allowed to adhere on the microdisk arrays for 12 h, and then unadhered cells were removed by medium exchange and the culture medium was supplemented with 0.18 mg/ml Matrigel. (*B*) Phase-contrast images of cyst arrays on the microdisk pattern on a glass substrate on day 4. The magnified image of a cyst on day 7 (inset) clearly shows the one-cell-thick cell wall and a lumen inside. (*C*) Confocal images of cysts on day 4 stained for nuclei (*blue*) and F-actin (*white*). Yellow dashed circles indicate microdisks without cysts and the blue color is autofluorescence of parylene. Scale bars: *B*, *C*, 50 μm; *B* inset, 20 μm.

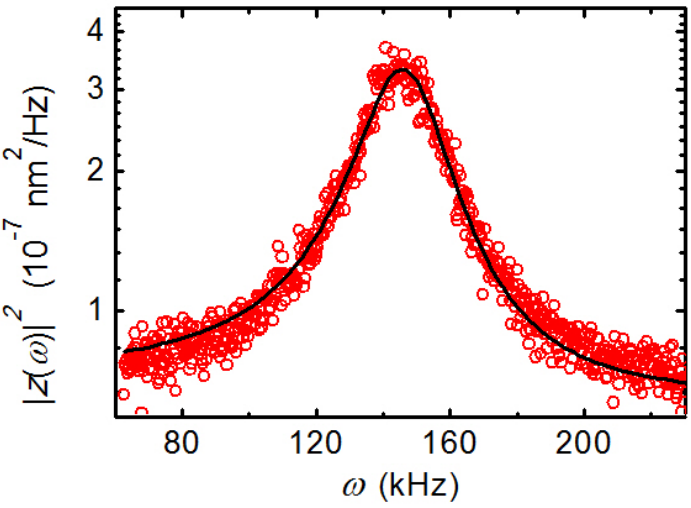

Figure S2 Measured power spectrum $|z(\omega)|^2$ as a function of angular frequency ω. The measurement was made when the colloidal probe immersed in the liquid buffer away from the cysts. The solid line is a fit to the theoretical function $|z(\omega)|^2 = \frac{2k_B T\xi / m^2}{(\omega_0^2 - \omega^2)^2 + (\omega\xi / m)^2}$ (4,5), with $m = 9.43\times10^{-8}$ g, $\omega_0 = 147.34$ kHz, and $\xi = 2.87\times10^{-6}$ Ns/m. The in situ spring constant of the colloidal probe was $k = m\omega_0^2 = 2.05$ N/m.

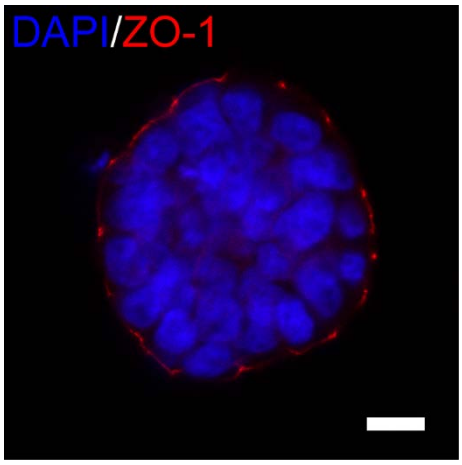

Figure S3 MDCK II cells cultured on microdisks formed spherical, concrete cell aggregates featuring an inverted polarity on day 3 and before. The image here is a confocal section through the middle of a cyst that was stained for nuclei (*blue*) and the tight junction protein ZO-1 (*red*). Scale bar: 10 μm.

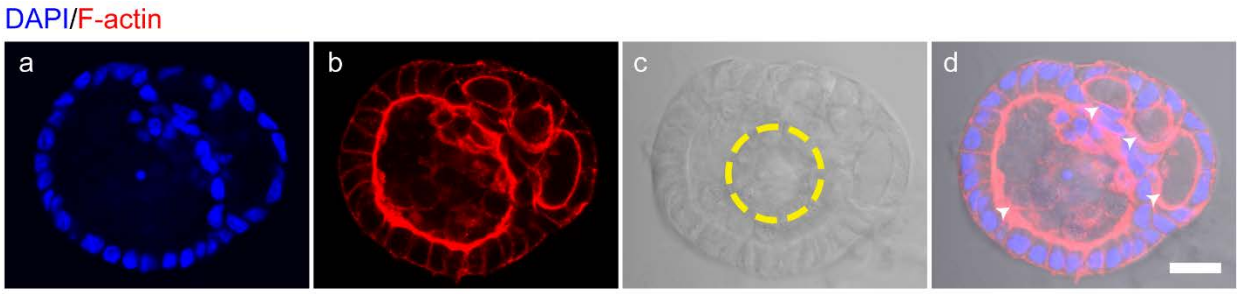

Figure S4 Multiple small lumens formed when cell polarity was not coordinated with cell proliferation due to a weak external apico-basal-polarization cue. Confocal images of an MDCK II cyst on a microdisk (*yellow dashed circle*); the cyst harbors multiple small lumens featuring normal polarity (*arrowheads*). The focal plane is at the middle of the cyst. Blue, nuclei; red, F-actin. Scale bar: 20 μm.

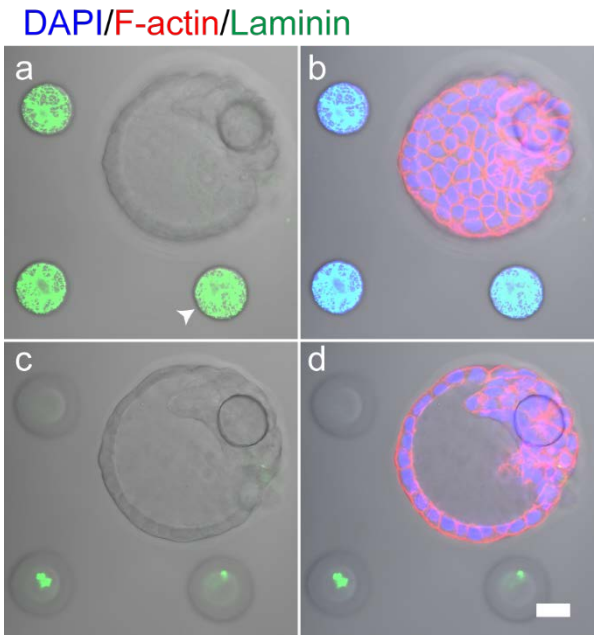

Figure S5 Exogenous laminin deposited on microdisks (*arrowhead*) was clearly detected, but no laminin was detected on the surface of day 4–5 cysts featuring an inverted polarity. The x-y sections in *b* and *d* are focused at the microplate-cyst interface and the top of the deposited laminin layer, respectively; *a* and *c*, show split views of *b* and *d*, respectively. Scale bars: 20 μm.

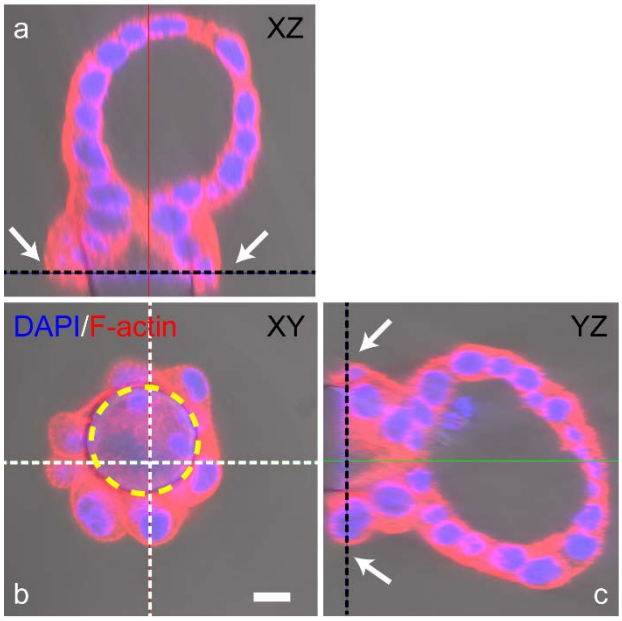

Figure S6 An MDCK II cyst grasping the 3-μm-raised microdisk by its cell protrusions (*white arrows*). Black dashed lines in *a* and *c* indicate the position of the x-y section in *b* which is focused at the cyst-microdisk interface, and white dashed lines in *b* indicate the corresponding positions of x-z (*a*) and y-z (*c*) sections of the cyst. Scale bar: 10 μm.

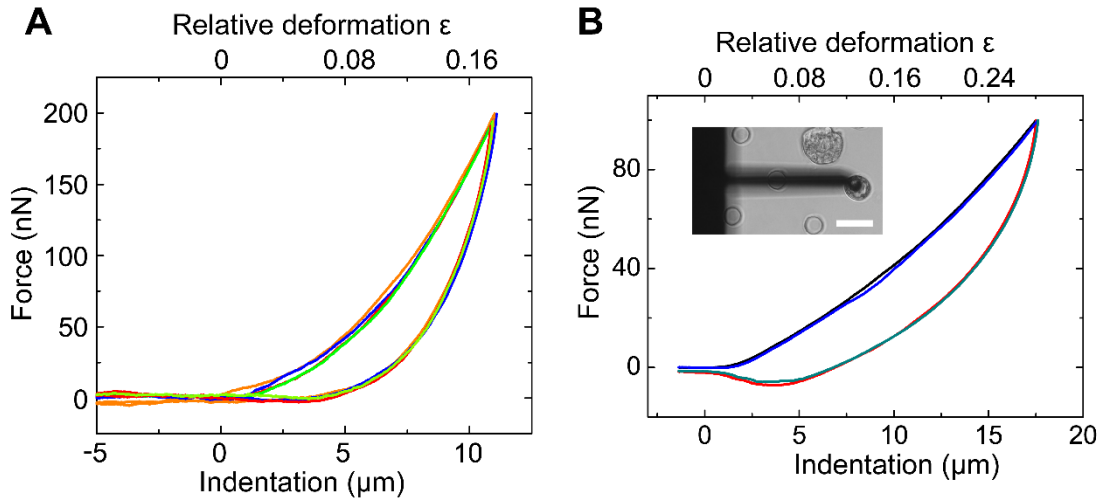

Figure S7 Force-distance curves measured for an MDCK II cyst and a pre-cyst. (*A*) A cyst was subjected to repetitive indentations with a 200 nN target force and a 1 μm/s indentation velocity. The force-distance curves were highly reproducible, as indicated by the overlapping colored curves. (*B*) Force-distance curves of 2 continuous measurements (*colored curves*) on a 3-day-old MDCK II pre-cyst. The inset shows a phase-contrast image of the pre-cyst under indentation. Scale bar: 50 μm.

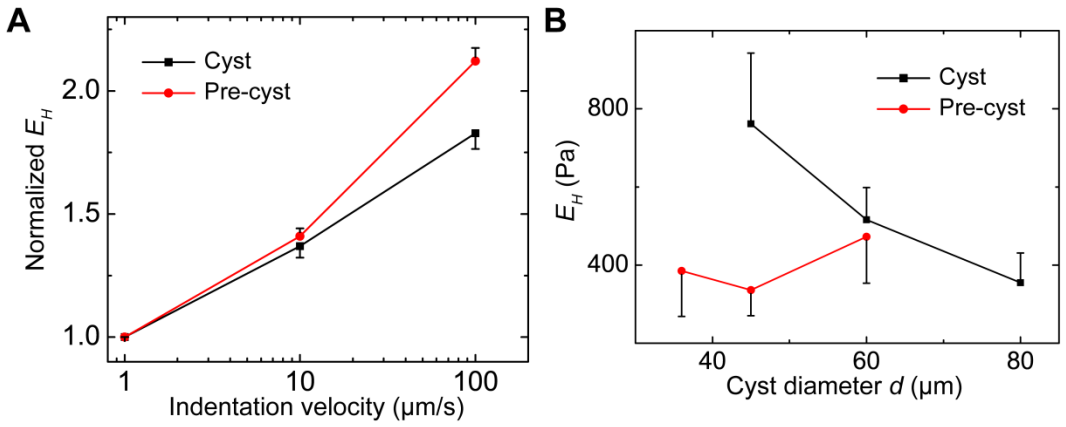

Figure S8 (*A*) Normalized Young's modulus E_H of MDCK II cysts (N = 7, n = 4) and pre-cysts (N = 15, n = 3) as a function of the indentation velocity, v, under indentation of F_M = 100 nN. The Young's modulus E_H of the cysts increased with v. (*B*) Young's modulus E_H of MDCK II cysts and pre-cysts as a function of cyst size under indentation of F_M = 100 nN and v = 1 μm/s. The moduli did not depend significantly on the size of the cysts (N = 4, 6, and 4, n = 6 for the 3 tested sizes; for cyst-diameter 45 and 80 μm groups, p = 0.084) or pre-cysts (N = 4, 8, and 3, n = 3).

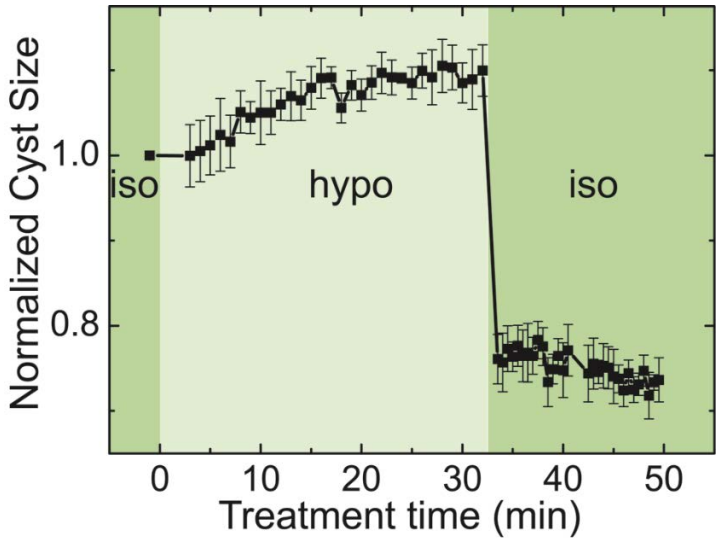

Figure S9 MDCK II cyst-size change upon consecutive hypotonic treatment (205 mOsm; *light green*) and isotonic treatment (320 mOsm; *dark green*). The cyst expanded gradually by ~10% within the 32-min hypotonic treatment and shrank by >20% of its initial size when the external buffering solution was changed back to the isotonic solution (n = 3). This asymmetric cyst-size change upon consecutive hypotonic and isotonic treatments suggested that the MDCK II cyst is a pressurized system.

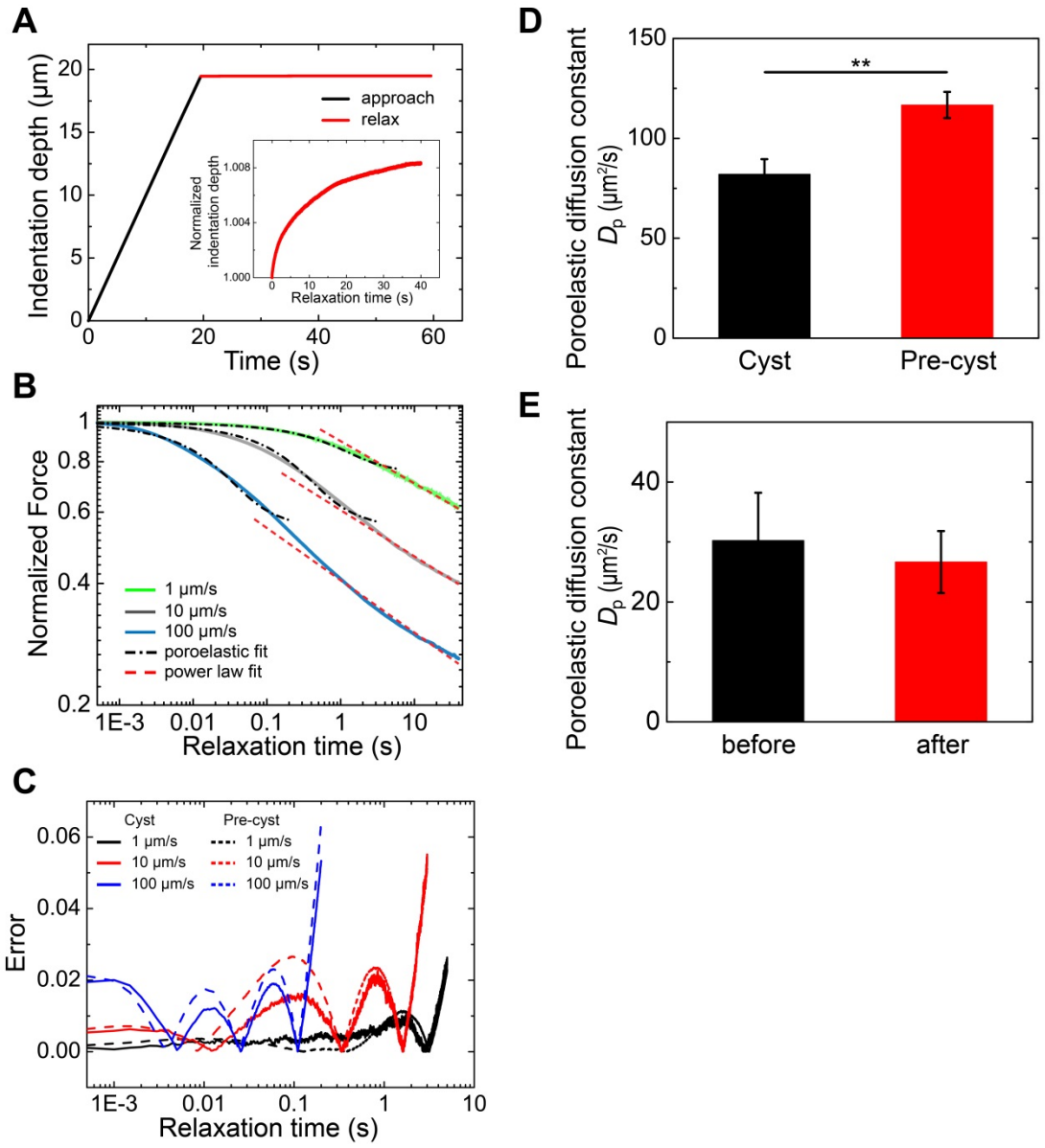

Figure S10 Stress-relaxation measurements on MDCK II cysts and pre-cysts and fitting-error comparison. (*A*) Typical temporal evolution of the indentation depth during the approach (*black*) and hold (*red*) processes. The inset shows the normalized indentation depth of the hold process which reveals that the indentation depth increased by <1% over the 40-s relaxation; this result suggests that the strain applied on the cysts was nearly constant during the force relaxation (*b* and *c* in Fig. 4 *A*). (*B*) Population-averaged force-relaxation curves obtained for MDCK II pre-cysts at various loading velocities (*shaded curves*). Curves are averages of N = 14, 15, and 15 MDCK II pre-cysts (n = 3) for loading velocities of v = 1, 10, and 100 μm/s, respectively. The dot-dashed lines and dashed lines show the fit of the experimental force relaxation with poroelastic and power-law relaxations, respectively. To obtain the best fitting for the poroelastic fit, we selected the first 6, 3, and 0.2 s of the averaged force relaxation under loading velocities of v = 1, 10, and 100 μm/s, respectively. R^2 = 0.963, 0.972, and 0.971, respectively. For the power-law fit, the ranges of the selected data were set as follows: relaxation time t = 6– 40, 3–40,

and 0.2–40 s, for v = 1, 10, and 100 μm/s, with power-law exponent β = 0.0986 ± 2.29 E-5, 0.111 ± 2.80 E-5, and 0.123 ± 5.20 E-5; R^2 = 0.996, 0.995, and 0.983, respectively. (*C*) Fitting error of the poroelastic model for cysts and pre-cysts at various loading velocities. The percentage error is defined as $|F(t) - F_{fit}|/F(t)$. (*D*) Poroelastic fitting of the experimental force-relaxation curves of MDCK II cysts and pre-cysts at a short timescale with a loading velocity of v =1 μm/s yielded a higher poroelastic diffusion coefficient (D_p) for the pre-cysts. N = 8 cysts (n = 4) and 12 pre-cysts (n = 4); p = 0.00301. (*E*) The poroelastic diffusion coefficient (D_p) obtained for MDCK II cysts did not differ significantly between before and after treatment with 0.1 μM $HgCl_2$; n = 5; p = 0.716.

Movie S1

A 6.5-h live imaging of rotating MDCK II cell aggregates on microdisks on day 7 of culture in conventional culture medium without Matrigel supplement. Images were captured at 1 frame/min. Scale bar: 30 μm.

Movie S2

One cycle of AFM cantilever approach and retraction for measuring force-distance curves. The blue dashed curves show the lumen outline before indentation, and the red curves show the outline when the target force, F_M, is reached. The cyst monolayer was slightly stretched during the indentation. Scale bar: 30 μm.

Movie S3

The cantilever loading procedure for stress-relaxation experiments on MDCK II cysts and pre-cysts; the procedure includes approach, hold, and retraction processes (1 each per cycle). Scale bar: 30 μm.

Supplementary references

1. Moeendarbary, E., L. Valon, M. Fritzsche, A. R. Harris, D. A. Moulding, A. J. Thrasher, E. Stride, L. Mahadevan, and G. T. Charras. 2013. The cytoplasm of living cells behaves as a poroelastic material. *Nat. Mater.* 12:253-261.
2. Hu, Y., X. Zhao, J. J. Vlassak, and Z. Suo. 2010. Using indentation to characterize the poroelasticity of gels. *Appl. Phys. Lett.* 96:121904.
3. Moeendarbary, E., and A. R. Harris. 2014. Cell mechanics: principles, practices, and prospects. *Wiley Interdiscip. Rev. Syst. Biol. Med.* 6:371-388.
4. Hutter, J. L., and Bechhoefer, J. 1993. Calibration of atomic force microscope tips. *Rev. Sci. Instrum.* 64:1868-1873.
5. Guan, D., Z. H. Hang, Z. Marcet, H. Liu, I. Kravchenko, C. Chan, H. Chan, and P. Tong. 2015. Direct Measurement of Optical Force Induced by Near-Field Plasmonic Cavity Using Dynamic Mode AFM. *Sci. Rep.* 5:16216.